Available online at www.sciencedirect.com
SCIENCE DIRECT®
International Journal of Solids and Structures 41 (2004) 7241–7265
INTERNATIONAL JOURNAL OF SOLIDS and STRUCTURES
www.elsevier.com/locate/ijsolstr

Time-harmonic BEM for 2-D piezoelectricity applied to eigenvalue problems

M. Denda [a,*], Y. Araki [b], Y.K. Yong [c]

[a] Department of Mechanical and Aerospace Engineering, Rutgers University, 98 Brett Road, Piscataway, NJ 08854-8058, USA
[b] Department of Architecture and Architectural Systems, Kyoto University, Sakyo, Kyoto 606-8501, Japan
[c] Department of Civil and Environmental Engineering, Rutgers University, 623 Bowser Road, Piscataway, NJ 08854-8014, USA

Received 21 June 2004
Available online 14 August 2004

Abstract

We will derive the fundamental generalized displacement solution, using the Radon transform, and present the direct formulation of the time-harmonic boundary element method (BEM) for the two-dimensional general piezoelectric solids. The fundamental solution consists of the static singular and the dynamics regular parts; the former, evaluated analytically, is the fundamental solution for the static problem and the latter is given by a line integral along the unit circle. The static BEM is a component of the time-harmonic BEM, which is formulated following the physical interpretation of Somigliana's identity in terms of the fundamental generalized line force and dislocation solutions obtained through the Stroh–Lekhnitskii (SL) formalism. The time-harmonic BEM is obtained by adding the boundary integrals for the dynamic regular part which, from the original double integral representation over the boundary element and the unit circle, are reduced to simple line integrals along the unit circle.

The BEM will be applied to the determination of the eigen frequencies of piezoelectric resonators. The eigenvalue problem deals with full non-symmetric complex-valued matrices whose components depend non-linearly on the frequency. A comparative study will be made of non-linear eigenvalue solvers: QZ algorithm and the implicitly restarted Arnoldi method (IRAM). The FEM results whose accuracy is well established serve as the basis of the comparison. It is found that the IRAM is faster and has more control over the solution procedure than the QZ algorithm. The use of the time-harmonic fundamental solution provides a clean boundary only formulation of the BEM and, when applied to the eigenvalue problems with IRAM, provides eigen frequencies accurate enough to be used for industrial applications. It supersedes the dual reciprocity BEM and challenges to replace the FEM designed for the eigenvalue problems for piezoelectricity.

Keywords: Piezoelectricity; 2-D time-harmonic dynamic problems; Direct formulation of boundary element method; Radon transform; Non-linear eigenvalue analysis by IRAM

* Corresponding author. Tel.: +1 732 4454391; fax: +1 732 4453124.
E-mail address: denda@jove.rutgers.edu (M. Denda).

0020-7683/$ - see front matter © 2004 Elsevier Ltd. All rights reserved.
doi:10.1016/j.ijsolstr.2004.06.052

1. Introduction

The time-harmonic boundary element method (BEM) in two-dimensions for the general piezoelectric solids is proposed in this paper. We will derive the fundamental solutions, formulate the direct BEM for the time-harmonic problems and apply it to the eigenvalue analysis. The motivation comes from the FEM (Wang et al., 1999) that faces the stiff computing requirements in the eigenvalue analysis of piezoelectric resonators. While the FEM must discretize the whole domain, the BEM models only the boundary and has the potential of reducing the computational burden of the FEM drastically. However, the BEM requires the fundamental displacement and traction solutions. For isotropic solids Kitahara (1985) has formulated the time-harmonic BEM for plates and 2-D elasticity problems using the time-harmonic fundamental solutions. For general anisotropic solids, Denda et al. (2003) have formulated the time-harmonic BEM in 2-D using the fundamental solutions obtained by Wang and Achenbach (1994). We will derive the 2-D time-harmonic fundamental solutions for piezoelectric solids using Radon transform and formulate the direct BEM. Norris (1994) also obtained the time-harmonic fundamental solution for piezoelectric (and anisotropic) solids without using Radon transform. The dual reciprocity boundary element method (DRBEM) of Nardini and Brebbia (1982) that uses much simpler static fundamental solution in the time-harmonic BEM and reduces the resulting volume integrals into boundary integrals does not provide accurate eigen frequency solutions (Kamiya et al., 1993) in higher frequency range as required in recent industry applications.

The fundamental solution for the general piezoelectric solids, as for the general anisotropic solids (Wang and Achenbach, 1994), can be split into static singular and dynamic regular parts; the former is given analytically and the latter is calculated numerically by the line integral along the unit circle. The former, being the fundamental solution of the static problem, results in the static BEM used either on its own for static problems or as a component of the time-harmonic BEM. In the formulation of the static BEM, following the physical interpretation of Somigliana's identity (Denda and Lua, 1999), we use the generalized line force and the generalized line dislocation solutions, which are obtained through the Stroh–Lekhnitskii (SL) formalism (Stroh, 1958; Lekhnitskii, 1963). We complete the formulation of the time-harmonic BEM by adding the boundary integrals for the dynamic regular part, which originally are double integrals: one over the unit semi-circle followed by another over the boundary element. The integrands of the double integrals are amenable to analytical evaluation over the boundary if performed before the integration over the unit circle. This is the trick we apply to reduce the double integrals to simple line integrals over the unit circle; the regularity of the integrands justifies this exchange operation.

Among a broad range of the time-harmonic BEM applications, we select the eigenvalue analysis. The resulting eigenvalue problem must deal with a full non-symmetric complex-valued matrix; each component depends non-linearly on the frequency. Kitahara (1985) used the direct (eigenvalue search) method to plot the variation of the determinant value as a function of the frequency. For solids of general anisotropy, Denda et al. (2003) divided the given frequency interval into sub-intervals and, for each sub-interval, approximated the components of the non-linear matrix by polynomials in the frequency to reduce the non-linear eigenvalue problem to the generalized linear eigenvalue problem to be solved by the QZ algorithm (Moler and Stewart, 1973). Although the accuracy of the QZ algorithm is superior, it is slow since the number of spurious eigen values rejected is high. The typical ratio of the numbers of non-spurious (accepted) and spurious (rejected) eigenvalues is 1 to NM, where N is the number of degrees of freedom of the problem and M (typically 1) is the order of polynomial approximation for the non-linear matrix in a given frequency interval.

The implicitly restarted Arnoldi method (IRAM) (Lehoucq et al., 1998), eliminating this waste, provides an accurate and dramatically faster eigen solver than the QZ algorithm. First, we will make a comparative study of these two non-linear eigenvalue solvers, while the FEM results whose accuracy is well established serve as the basis of the comparison. Although the eigen frequencies sought in the sub-interval of frequency

are real-valued, the IRAM produces spurious eigen frequencies which have the large imaginary part or the real part outside the sub-interval. Even for the legitimate eigen frequency, its imaginary part may not be perfectly zero due to the error introduced by the polynomial approximation and by the boundary element discretization. Hence, after solving the linear eigenvalue problem, a procedure to select the eigenvalues with the imaginary part less than a specified tolerance and the real part within the sub-interval is required. Use of a tight tolerance for the imaginary part and a very small sub-interval size will satisfy the accuracy requirements well into the higher frequency range. We will perform a series of numerical experiments with the piezoelectric solid in 2-D to assess the optimum tolerance size for the imaginary part, the sub-interval size, and the boundary element mesh for the required level of accuracy of the eigen frequency.

The proposed BEM implementation combined with the non-linear eigenvalue solver IRAM provides a reliable platform for the computation of eigen frequencies for the general piezoelectric solids. The use of the time-harmonic fundamental solution provides a clean boundary only formulation of the BEM. It supersedes the double reciprocity BEM (DRBEM) and challenges to replace the FEM designed for the eigenvalue analysis. More important, the proposed BEM is generally applicable to a wider class of two-dimensional piezoelectric time-harmonic problems not limited to the eigenvalue analysis.

2. Time-harmonic piezoelectricity in 2-D

2.1. Basic equations

Consider the two-dimensional elastodynamic problem in piezoelectric solid, where the field quantities depend only on the coordinates x_1 and x_2. Let $\mathbf{x}$ and t indicate the two-dimensional position vector (x_1, x_2) and time, respectively. Under the electrostatic approximation, the equations of motion and the Gauss's law in terms of the displacement u_i, the electric potential φ, the body force f_i, mass density ρ, and the charge density ρ_e are given by

$$c_{i\alpha j\beta}u_{j,\beta\alpha} + e_{\beta i\alpha}\varphi_{,\beta\alpha} - \rho\partial_t^2 u_i = -f_i, \tag{1}$$

$$e_{\alpha j\beta}u_{j,\beta\alpha} - \kappa_{\alpha\beta}\varphi_{,\beta\alpha} = \rho_e, \tag{2}$$

where the c_{ijpq}, e_{ijk} and κ_{ij} are the elastic stiffness, the piezoelectric stress and the dielectric permittivity constants, respectively. The Greek and lowercase Roman subscripts range from 1 to 2 and 1 to 3, respectively; a repeated index is summed over its full range. We denote the derivative with respect to x_α of a function $\mathscr{F}$ by $\mathscr{F}_{,\alpha}$ or $\partial_\alpha\mathscr{F}$, while its time derivative by $\partial_t\mathscr{F}$. If we introduce

$$U_J = \begin{cases} u_J & (J = 1,2,3), \\ \varphi & (J = 4), \end{cases}$$

$$E_{I\alpha J\beta} = \begin{cases} c_{I\alpha J\beta} & (I,J = 1,2,3), \\ e_{\beta I\alpha} & (J = 4, I = 1,2,3), \\ e_{\alpha J\beta} & (I = 4, J = 1,2,3), \\ -\kappa_{\alpha\beta} & (I = J = 4), \end{cases}$$

$$\rho_{IJ} = \begin{cases} \rho & (I = J = 1,2,3), \\ 0 & (I = J = 4 \text{ or } I \neq J), \end{cases}$$

$$F_J = \begin{cases} f_J & (J = 1,2,3), \\ -\rho_e & (J = 4), \end{cases}$$

then we can combine (1) and (2) to get the generalized equations of motions

$$E_{I\alpha J\beta} U_{J,\beta\alpha} - \rho_{IJ} \partial_t^2 U_J = -F_I, \tag{3}$$

where U_J and F_J are the generalized displacement and body force. Note that the uppercase Roman indices range from 1 to 4. Introduce the generalized stress and traction

$$\begin{aligned} \Sigma_{\alpha J} &= \begin{cases} \sigma_{\alpha J} & (J = 1,2,3), \\ D_\alpha & (J = 4), \end{cases} \\ T_J &= \begin{cases} t_J & (J = 1,2,3), \\ -\omega_e & (J = 4), \end{cases} \end{aligned} \tag{4}$$

where $\sigma_{\alpha J}$ and D_α are the stress and electric induction components, respectively, with t_J and ω_e being the traction component and the surface charge density, respectively. They are related by

$$T_J = v_\alpha \Sigma_{\alpha J} = v_\alpha E_{\alpha JP\beta} U_{P,\beta}, \tag{5}$$

where v_α is the unit normal component.

Consider an infinite piezoelectric solid subjected, at the origin and at time $t = -\infty$, to a time-harmonic generalized line force in the x_K-direction given by

$$F_I(\mathbf{x}, t) = \delta_{IK} \delta(\mathbf{x}) \mathrm{e}^{-\mathrm{i}\omega t}, \tag{6}$$

where $i = \sqrt{-1}$, δ_{IK} is Kronecker delta and ω is the angular frequency. The resulting generalized displacement is in steady state motion and written as

$$U_{IK}(\mathbf{x}, t) = G_{IK}(\mathbf{x}, \omega) \mathrm{e}^{-\mathrm{i}\omega t}, \tag{7}$$

where $G_{IK}(\mathbf{x}, \omega)$ is the fundamental solution with the physical interpretations:

$G_{ik}(\mathbf{x}, \omega)$ Elastic displacement in the x_i-direction at $\mathbf{x}$ and t due to a line force in the x_k-direction at the origin;
$G_{i4}(\mathbf{x}, \omega)$ Elastic displacement in the x_i-direction at $\mathbf{x}$ and t due to a line charge at the origin;
$G_{4k}(\mathbf{x}, \omega)$ Electric potential at $\mathbf{x}$ and t due to a line force in the x_k-direction at the origin; and
$G_{44}(\mathbf{x}, \omega)$ Electric potential at $\mathbf{x}$ and t due to a line charge at the origin.

Substitute (6) and (7) into (3) and omit the time factor $e^{-\mathrm{i}\omega t}$ to get

$$\left\{ \Gamma_{IJ}(\partial_1, \partial_2) + \rho_{IJ} \omega^2 \right\} G_{JK}(\mathbf{x}, \omega) = f - \delta_{IK} \delta(\mathbf{x}), \tag{8}$$

where

$$\Gamma_{IJ}(\partial_1, \partial_2) = E_{I\alpha J\beta} \partial_\alpha \partial_\beta. \tag{9}$$

The basis of the direct formulation of the boundary element method for time-harmonic dynamic piezoelectricity is the generalized Somigliana's identity

$$U_K(\mathbf{x}, \omega) = \int_{\partial A} T_I(\mathbf{x}, \omega) G_{IK}(\mathbf{y} - \mathbf{x}, \omega) \mathrm{d}l(\mathbf{y}) - \int_{\partial A} U_I(\mathbf{x}, \omega) H_{IK}(\mathbf{y} - \mathbf{x}, \omega; \mathbf{v}) \mathrm{d}l(\mathbf{y}), \tag{10}$$

where $H_{IK}(\mathbf{y} - \mathbf{x}, \omega; \mathbf{v})$ is Ith component the generalized traction at $\mathbf{y}$ corresponding to the generalized line force in the x_K-direction at $\mathbf{x}$ and given by

$$H_{IK}(\mathbf{y}-\mathbf{x},\omega;\mathbf{v}) = v_\alpha(\mathbf{y})E_{\alpha IP\beta}G_{PK,\beta}(\mathbf{y}-\mathbf{x},\omega), \tag{11}$$

where $v_\alpha(\mathbf{y})$ is the unit normal component on the boundary ∂A.

2.2. Fundamental solutions by radon transform

The Radon transform of an arbitrary function $f(\mathbf{x})$ is defined (Wang and Achenbach, 1994) as

$$\hat{f}(s,\mathbf{n}) = \int f(\mathbf{x})\delta(s,\mathbf{n}\cdot\mathbf{x})\mathrm{d}\mathbf{x},$$

which is an integration of $f(\mathbf{x})$ along a line $\mathbf{n}\cdot\boldsymbol{x}=s$, defined by a unit vector $\mathbf{n}=(n_1,n_2)$ and a scalar s, in two-dimensions. The inverse Radon transform is defined by

$$f(\mathbf{x}) = \int_{|\mathbf{n}|=1} \bar{f}(\mathbf{n}\cdot\mathbf{x},\mathbf{n})\mathrm{d}\mathbf{n}, \tag{12}$$

where

$$\bar{f}(s,\mathbf{n}) = \frac{1}{4\pi^2}\int_{-\infty}^{\infty}\frac{\partial_\sigma\hat{f}(\sigma,\mathbf{n})}{s-\sigma}\mathrm{d}\sigma.$$

The integral in (12) is a line integral over a unit circle.

Apply the Radon transform to (8) to get

$$\left\{\Gamma_{IJ}(\mathbf{n})\partial_s^2+\rho_{IJ}\omega^2\right\}\widehat{G}_{JK}(\mathbf{x},\omega) = -\delta_{IK}\delta(s), \tag{13}$$

which consists of four groups of equations

$$\Gamma_{ij}(\mathbf{n})\partial_s^2\widehat{G}_{jk}+\Gamma_{i4}(\mathbf{n})\partial_s^2\widehat{G}_{4k}+\rho\omega^2\widehat{G}_{ik} = -\delta_{ik}\delta(s), \tag{14}$$

$$\Gamma_{ij}(\mathbf{n})\partial_s^2\widehat{G}_{j4}+\Gamma_{i4}(\mathbf{n})\partial_s^2\widehat{G}_{44}+\rho\omega^2\widehat{G}_{i4} = 0, \tag{15}$$

$$\Gamma_{4j}(\mathbf{n})\partial_s^2\widehat{G}_{jk}+\Gamma_{44}(\mathbf{n})\partial_s^2\widehat{G}_{4k} = 0, \tag{16}$$

$$\Gamma_{4j}(\mathbf{n})\partial_s^2\widehat{G}_{j4}+\Gamma_{44}(\mathbf{n})\partial_s^2\widehat{G}_{44} = -\delta(s), \tag{17}$$

where

$$\Gamma_{IJ}(\mathbf{n}) = E_{I\alpha J\beta}n_\alpha n_\beta. \tag{18}$$

We recall that the lowercase Roman indices i, j and k range from 1 to 3.

Use (16) to eliminate $\widehat{G}_{4k}$ in (14) to get a system of ordinary differential equations involving only $\widehat{G}_{jk}$,

$$L_{ij}(\mathbf{n})\partial_s^2\widehat{G}_{jk}+\rho\omega^2\widehat{G}_{ik} = -\delta_{ik}\delta(s), \tag{19}$$

where

$$L_{ij}(\mathbf{n}) = L_{ij}(n_1,n_2) = \Gamma_{ij}(\mathbf{n})-\frac{\Gamma_{i4}(\mathbf{n})\Gamma_{4j}(\mathbf{n})}{\Gamma_{44}(\mathbf{n})}, \tag{20}$$

is symmetric and positive definite. We follow Wang and Achenbach (1994) for the derivation of $\widehat{G}_{jk}$ from (19); definitions and equations used in the derivation are

(A) Eigen equations for the matrix $L_{ij}(\mathbf{n})$

$$L_{ij}(\mathbf{n})V_{jm} = \lambda_m V_{im} \quad (m=1,2,3;\quad \text{no sum on } m), \tag{21}$$

where λ_m and V_{im} are the eigenvalues and eigenvectors of the matrix $L_{ij}(\mathbf{n})$.

(B) Adjoint matrix

$$E^m_{jk} = \mathrm{adj}[L_{jk}(\mathbf{n}) - \lambda_m \delta_{jk}] \quad (m = 1, 2, 3). \tag{22}$$

(C) The phase velocity v_m and wave number k_m

$$v_m = \sqrt{\frac{\lambda_m}{\rho}}, \quad k_m = \frac{\omega}{v_m} \quad (m = 1, 2, 3). \tag{23}$$

Notice that other components, $\widehat{G}_{4k}$ and $\widehat{G}_{44}$, of the fundamental solution are given in terms of $\widehat{G}_{jk}$ through (16) and (17). After applying the inverse Radon transform to $\widehat{G}_{JK}$, we get the fundamental solution G_{JK}, which can be expressed by a sum of static singular part G^{S}_{JK} and dynamic regular part G^{R}_{JK} as

$$G_{JK}(\mathbf{x}, \omega) = G^{\mathrm{S}}_{JK}(\mathbf{x}) + G^{\mathrm{R}}_{JK}(\mathbf{x}, \omega). \tag{24}$$

2.2.1. Static singular part

Define the adjoint and determinant of 4×4 matrix $\Gamma_{JK}(1,\eta)$

$$F_{JK}(\eta) = \mathrm{adj}[L_{JK}(1, \eta)], \quad D(\eta) = \det[\Gamma_{JK}(1, \eta)]. \tag{25}$$

Then, the static singular part in (24) is given by

$$G^{\mathrm{S}}_{JK}(\mathbf{x}) = \mathscr{G}^{\mathrm{S}}_{JK}(\mathbf{x}) + C_{JK} \tag{26}$$

with

$$\mathscr{G}^{\mathrm{S}}_{JK}(\mathbf{x}) = \frac{1}{\pi} \Im \sum_{M=1}^{4} \frac{F_{JK}(\eta_M)}{\partial_\eta D(\eta_M)} \log(z_M) \tag{27}$$

and

$$C_{JK} = -\frac{1}{\pi} \Im \sum_{M=1}^{4} \frac{F_{JK}(\eta_M)}{\partial_\eta D(\eta_M)} \log(\eta_M + i), \tag{28}$$

where

$$z_M = x_1 + \eta_M x_2 \quad (M = 1, 2, 3, 4), \tag{29}$$

are generalized complex variables and η_M ($M = 1,2,3,4$ with $\Im(\eta_M) > 0$) are four distinct roots of the eighth-order characteristic polynomial

$$D(\eta) = 0, \tag{30}$$

which has four conjugate pairs of roots $(\eta_M, \bar{\eta}_M)$. The symbol $\Im$ indicates the imaginary part of a complex variable. Without loss of generality, we assume four distinct roots in this paper. The static singular part $G^{\mathrm{S}}_{JK}(\mathbf{x})$ in the left-hand side of (26) is the static fundamental solution obtained by Wang (1996). Note that $\mathscr{G}^{\mathrm{S}}_{JK}(\mathbf{x})$ differs from $G^{\mathrm{S}}_{JK}(\mathbf{x})$ by the constant term C_{JK}. These constants are inessential in the formulation of the elastostatic BEM, but they are required for the time-harmonic dynamic BEM.

2.2.2. Dynamic regular part

The dynamic regular part in (24) is given by

$$G^{\mathrm{R}}_{JK}(\mathbf{x}, \omega) = \int_{|\mathbf{n}|=1} \overline{G}^{\mathrm{R}}_{JK}(\mathbf{n} \cdot \mathbf{x}, \mathbf{n}) \mathrm{d}\mathbf{n}, \tag{31}$$

where

$$\overline{G}^{\mathrm{R}}_{JK}(\mathbf{n}\cdot\mathbf{x},\mathbf{n}) = \frac{1}{8\pi^2}\sum_{m=1}^{3}\frac{\mathscr{E}^{m}_{JK}}{\rho c_m^2 E^{m}_{qq}}\phi^{\mathrm{R}}(k_m|\mathbf{n}\cdot\mathbf{x}|) \tag{32}$$

with

$$\mathscr{E}^{m}_{JK} = \begin{cases} E^{m}_{JK} & J,K = 1,2,3, \\ -\frac{F^{m}_{Ji}\Gamma_{i4}(\mathbf{n})}{\Gamma_{44}(\mathbf{n})} & J = 1,2,3; K = 4 \\ \frac{F^{m}_{qp}\Gamma_{4q}(\mathbf{n})\Gamma_{p4}(\mathbf{n})}{\Gamma^2_{44}(\mathbf{n})} & J = K = 4 \end{cases} \tag{33}$$

and the case $K = 1,2,3$ and $J = 4$ is covered by the symmetry property $\mathscr{E}^{m}_{JK} = \mathscr{E}^{m}_{KJ}$. Note that the indices i, p and q in (33) are summed over 1 to 3. The function $\phi^{R}(k_m|\mathbf{n}\cdot\mathbf{x}|)$ is defined by

$$\phi^{\mathrm{R}}(k_m|\mathbf{n}\cdot\mathbf{x}|) = \phi(k_m|\mathbf{n}\cdot\mathbf{x}|) + 2\log|\mathbf{n}\cdot\mathbf{x}| \tag{34}$$

with

$$\phi(\zeta) = \mathrm{i}\pi e^{\mathrm{i}\zeta} - 2[\cos(\zeta)\mathrm{ci}(\zeta) + \sin(\zeta)\mathrm{si}(\zeta)], \tag{35}$$

where $\mathrm{ci}(\zeta)$ and $\mathrm{si}(\zeta)$ are the sine and cosine integral functions; the logarithmic function in the right hand side of (34) is added to cancel the singularity of $\phi(k_m|\mathbf{n}\cdot\mathbf{x}|)$ at the origin. Without loss of generality, we assume three distinct c_m in (32); special formulas for coincident cases are provided by Wang and Achenbach (1994).

Substitute (31) into (5) to get the corresponding generalized traction contribution of the dynamic regular part, given by

$$H^{\mathrm{R}}_{JK}(\mathbf{x},\omega;\mathbf{v}) = \int_{|\mathbf{n}|=1}\overline{H}^{\mathrm{R}}_{JK}(\mathbf{n}\cdot\mathbf{x},\mathbf{n};\mathbf{v})\,\mathrm{d}\mathbf{n}, \tag{36}$$

where

$$\overline{H}^{\mathrm{R}}_{JK}(\mathbf{n}\cdot\mathbf{x},\mathbf{n};\mathbf{v}) = \frac{1}{8\pi^2}\mathrm{sign}(\mathbf{n}\cdot\mathbf{x})\sum_{m=1}^{3}\frac{1}{\rho c_m^2}\frac{\mathscr{E}^{*m}_{JK}}{E^{m}_{qq}}\phi^{\mathrm{R}\prime}(k_m|\mathbf{n}\cdot\mathbf{x}|) \tag{37}$$

with

$$\mathscr{E}^{*m}_{JK} = \gamma_{JR}E^{m}_{RK}, \quad \gamma_{JR} = v_\alpha E_{\alpha JR\beta}n_\beta, \tag{38}$$

and the prime attached to the function such as

$$\phi^{\mathrm{R}\prime}(k_m|\mathbf{n}\cdot\mathbf{x}|) = k_m\phi'(k_m|\mathbf{n}\cdot\mathbf{x}|) + 2\log'(|\mathbf{n}\cdot\mathbf{x}|), \tag{39}$$

indicates the derivative with respect to its argument. Repeated indices R and α and β in (38) should be summed over the ranges 1 to 4 and 1 to 2, respectively.

3. Static piezoelectricity in 2-D

In the formulation of the static BEM, following the physical interpretation of Somigliana's identity (Denda and Lua, 1999), we will use the displacement solutions for the generalized line force and the generalized dislocation dipoles; the generalized Stroh formalism provides the framework for their derivation. In the generalized Stroh formalism for 2-D piezoelectricity the generalized displacement U_I and force resultant R_I are given in the form

$$U_I = 2\Re\left\{\sum_{J=1}^{4} A_{IJ} f_J(z_J)\right\}, \quad R_I = -2\Re\left\{\sum_{J=1}^{4} L_{IJ} f_J(z_J)\right\}, \tag{40}$$

where A_{IJ} and L_{IJ} are the components of 4×4 complex valued matrices $\mathbf{L}$ and $\mathbf{A}$ defined later by Eq. (44)–(47). Each of four functions $f_J(z_J)$, $(J = 1,2,\ldots,4)$ is analytic in its argument $z_J = x_1 + \eta_J x_2$. Here η_J are four distinct complex numbers which, along with their four conjugates, are the roots of the eighth-order polynomial characteristic equations in η,

$$\begin{aligned} &d^{(4)}(\eta)d^{(2)}(\eta)f^{(2)}(\eta) + d^{(4)}(\eta)\mathrm{e}^{(2)}(\eta)\mathrm{e}^{(2)}(\eta) - d^{(3)}(\eta)d^{(3)}(\eta)f^{(2)}(\eta) - 2d^{(3)}(\eta)\mathrm{e}^{(3)}(\eta)\mathrm{e}^{(2)}(\eta) \\ &\quad + d^{(2)}(\eta)\mathrm{e}^{(3)}(\eta)\mathrm{e}^{(3)}(\eta) = 0, \end{aligned} \tag{41}$$

where

$$\begin{aligned} d^{(4)}(\eta) &= S_{11}\eta^4 - 2S_{16}\eta^3 + (2S_{12} + S_{66})\eta^2 - 2S_{26}\eta + S_{22}, \\ d^{(3)}(\eta) &= S_{15}\eta^3 - (S_{14} + S_{56})\eta^2 + (S_{25} + S_{46})\eta - S_{24}, \\ \mathrm{e}^{(3)}(\eta) &= G_{11}\eta^3 - (G_{21} + G_{16})\eta^2 + (G_{12} + G_{26})\eta - G_{22}, \\ d^{(2)}(\eta) &= S_{55}\eta^2 - 2S_{45}\eta + S_{44}, \\ \mathrm{e}^{(2)}(\eta) &= G_{15}\eta^2 - (G_{14} + G_{25})\eta + G_{24}, \\ f^{(2)}(\eta) &= B_{11}\eta^2 - 2B_{12}\eta + B_{22}. \end{aligned} \tag{42}$$

The coefficients $S_{\mathscr{M}\mathscr{N}}$, $G_{\alpha\mathscr{N}}$ and $B_{\alpha\beta}$ are reduced elastic compliance, reduced piezoelectric strain and reduced dielectric impermeability constants, respectively, given by

$$\begin{aligned} S_{\mathscr{M}\mathscr{N}} &= s_{\mathscr{M}\mathscr{N}} - \frac{s_{\mathscr{M}3}s_{\mathscr{N}3}\beta_{33} + (s_{\mathscr{M}3}g_{3\mathscr{N}} + s_{\mathscr{N}3}g_{3\mathscr{M}})g_{33} - g_{3\mathscr{M}}g_{3\mathscr{N}}s_{33}}{s_{33}\beta_{33} + g_{33}^2}, \\ G_{\alpha\mathscr{M}} &= g_{\alpha\mathscr{M}} - \frac{s_{\mathscr{M}3}g_{\alpha3}\beta_{33} + (-s_{M3}\beta_{\alpha3} + g_{3\mathscr{M}}g_{\alpha3})g_{33} + g_{3\mathscr{M}}\beta_{\alpha3}s_{33}}{s_{33}\beta_{33} + g_{33}^2}, \\ B_{\alpha\beta} &= \beta_{\alpha\beta} + \frac{g_{\alpha3}g_{\beta3}\beta_{33} - (g_{\alpha3}\beta_{\beta3} + g_{\beta3}\beta_{\alpha3})g_{33} - \beta_{\alpha3}\beta_{\beta3}s_{33}}{s_{33}\beta_{33} + g_{33}^2}, \\ &(\mathscr{M},\mathscr{N} = 1,2,4,5,6;\alpha,\beta = 1,2) \end{aligned} \tag{43}$$

in terms of the elastic compliance ($s_{\mathscr{M}\mathscr{N}}$ with $\mathscr{M},\mathscr{N} = 1,2,3,4,5,6$), piezoelectric strain ($g_{i\mathscr{M}}$ with $i = 1,2,3$ and $\mathscr{M} = 1,2,3,4,5,6$) and dielectric impermeability (β_{ik} with $i,k = 1,2,3$) constants, respectively. Notice that, for the elastic compliance and the piezoelectric strain constants, each pair of suffices ij is replaced by one suffix following the convention $(11 \to 1)$, $(22 \to 2)$, $(33 \to 3)$, $(23 \to 4)$, $(31 \to 5)$ and $(12 \to 6)$.

The 4×4 matrix $\mathbf{L}$ is defined by

$$\mathbf{L} = [\mathbf{L}_1, \mathbf{L}_2, \mathbf{L}_3, \mathbf{L}_4] = \begin{bmatrix} -\eta_1 L_{21} & -\eta_2 L_{22} & -\eta_3 l_3 L_{33} & -\eta_4 l_7 L_{44} \\ L_{21} & L_{22} & l_3 L_{33} & l_7 L_{44} \\ l_1 L_{21} & l_2 L_{22} & L_{33} & l_8 L_{44} \\ l_4 L_{21} & l_5 L_{22} & l_6 L_{33} & L_{44} \end{bmatrix}, \tag{44}$$

where

$$l_\alpha = \frac{[f^{(2)}d^{(3)} + e^{(2)}e^{(3)}](\eta_\alpha)}{[d^{(2)}f^{(2)} + e^{(2)}e^{(2)}](\eta_\alpha)} \quad (\alpha = 1,2) \qquad l_3 = \frac{[f^{(2)}d^{(3)} + e^{(3)}e^{(2)}](\eta_3)}{[d^{(4)}f^{(2)} + e^{(3)}e^{(3)}](\eta_3)},$$
$$l_\beta = \frac{[e^{(2)}d^{(3)} - d^{(2)}e^{(3)}](\eta_\alpha)}{[d^{(2)}f^{(2)} + e^{(2)}e^{(2)}](\eta_\alpha)} \quad (\beta = 4,5; \alpha = 1,2) \qquad l_6 = \frac{[d^{(4)}e^{(2)} - d^{(3)}e^{(3)}](\eta_3)}{[d^{(4)}f^{(2)} + e^{(3)}e^{(3)}](\eta_3)}, \tag{45}$$
$$l_7 = \frac{[d^{(2)}e^{(3)} - d^{(3)}e^{(2)}](\eta_4)}{[d^{(4)}d^{(2)} - d^{(3)}d^{(3)})](\eta_4)} \qquad l_8 = \frac{[d^{(3)}e^{(3)} - d^{(4)}e^{(2)}](\eta_4)}{[d^{(4)}d^{(2)} - d^{(3)}d^{(3)}](\eta_4)}$$

and the 4×4 matrix $\mathbf{A}$ by

$$\mathbf{A} = [\mathscr{A}_1\mathbf{L}_1, \mathscr{A}_2\mathbf{L}_2, \mathscr{A}_3\mathbf{L}_3, \mathscr{A}_4\mathbf{L}_4], \tag{46}$$

where

$$\mathscr{A}_M = \begin{bmatrix} S_{16} - S_{11}\eta_M, & S_{12}, & S_{14} - S_{15}\eta_M, & G_{21} - G_{11}\eta_M \\ \dfrac{S_{26} - S_{21}\eta_M}{\eta_M}, & \dfrac{S_{22}}{\eta_M}, & \dfrac{S_{24} - S_{25}\eta_M}{\eta_M}, & \dfrac{G_{22} - G_{12}\eta_M}{\eta_M} \\ S_{56} - S_{51}\eta_M, & S_{52}, & S_{54} - S_{55}\eta_M, & G_{25} - G_{15}\eta_M \\ G_{16} - G_{11}\eta_M, & G_{12}, & G_{14} - G_{15}\eta_M, & -B_{12} + B_{11}\eta_M \end{bmatrix}. \tag{47}$$

The two matrices are normalized by the relation

$$2\sum_{I=1}^{4} L_{IM}A_{IM} = 1 \quad (M = 1,2,3,4). \tag{48}$$

Consider a unit Kth component of the generalized line force at the origin; the resulting Jth component of the generalized displacement $\mathscr{G}^{\mathrm{S}}_{JK}(z)$ is given by

$$\mathscr{G}^{\mathrm{S}}_{JK}(z) = \Im\frac{1}{\pi}\sum_{M=1}^{4} A_{JM}A_{KM}\log(z_M), \tag{49}$$

where $z = x_1 + \mathrm{i}x_2$ and $z_M = x_1 + \eta_M x_2$. Next consider a unit Kth component of the generalized dislocation dipole at the origin along a segment $\mathrm{d}\xi = \mathrm{d}y_1 + \mathrm{i}\,\mathrm{d}y_2$ of length $\mathrm{d}s$, which is a segment of the generalized displacement discontinuity; the resulting Jth component of the generalized displacement $G^{(d)}_{JK}(z)\,\mathrm{d}s$ is given by

$$G^{(d)}_{JK}(z)\,\mathrm{d}s = -\Im\frac{1}{\pi}\sum_{M=1}^{4} A_{JM}L_{KM}\frac{\mathrm{d}\xi_M}{z_M}, \tag{50}$$

where $\mathrm{d}\xi_M = \mathrm{d}y_1 + \eta_M\mathrm{d}y_2$. Formulas (49) and (27) provide two alternative and equivalent expressions for the static generalized displacement fundamental solution, while formula (50) coincides with the minus of the static generalized traction fundamental solution of the generalized line force.

4. Direct formulation of the BEM

As the time-harmonic fundamental solution is split into static singular and dynamic regular parts, so is the numerical implementation of the boundary elements: the static singular boundary element (SSBE) and the dynamic regular boundary element (DRBE) implementations. While the SSBE alone can solve static problems, the time-harmonic BEM requires both components.

4.1. Static singular boundary element

The kernel functions H_{IK} in the generalized Somigliana's identity (10) has two interpretations (Denda and Lua, 1999): (1) the generalized traction due to the generalized line force and (2) the generalized displacement due to the generalized dislocation dipole. The second definitions leads to the physical interpretation of the generalized Somigliana's identity: the generalized displacement field in a domain A can be represented by continuous distributions of the generalized line forces (F_I) and dislocation dipoles (U_I) along the contour ∂A in an infinite body that coincides with the boundary of the domain, where F_I and U_I are the magnitudes of the generalized traction and displacement on the boundary. Stroh–Lekhnitskii formalism provides an ideal platform for the derivation of the generalized line force and dislocation solutions; it uses four generalized complex variables $z_M = x_1 + \eta_M x_2$ ($M = 1,2,3,4$) based on the coordinates (x_1, x_2) and the four roots η_M of the characteristic polynomial (41).

We approximate the whole boundary by a collection of straight elements $\sum_\Gamma$. Consider a boundary element Γ of length L with the end (1,2) and the middle three nodes; introduce four generalized complex variables $\xi_M = y_1 + \eta_M\, y_2 (M = 1,2,3,4)$ based on the coordinates (y_1, y_2) of the source point on the element. Approximate the generalized displacement and traction on the boundary by quadratic interpolation functions:

$$U_J(\xi_M) = \sum_{a=1}^{3} \varphi_a(\xi_M) U_J^a, \quad T_j(\xi_M) = \sum_{a=1}^{3} \varphi_a(\xi_M) T_J^a, \tag{51}$$

where $\varphi_n(\xi_M)$ ($a = 1,2,3$) are the quadratic shape functions and U_J^a and T_J^a are the nodal values of U_J and T_j. The shape functions are given by

$$\varphi_a(\xi_M) = \frac{\left(\xi_M - \xi_M^b\right)\left(\xi_M - \xi_M^c\right)}{\left(\xi_M^a - \xi_M^b\right)\left(\xi_M^a - \xi_M^c\right)} \quad (a = 1,2,3 \text{ and } b \neq c \neq a), \tag{52}$$

where ξ_M^a ($a = 1,2,3$) are nodal values of the generalized complex variables ξ_M; no summation is taken over the repeated indices. The pth derivative, with respect to ξ_M, of the interpolation functions (51) are given by

$$U_J^{(p)}(\xi_M) = \sum_{a=1}^{3} \varphi_a^{(p)}(\xi_M) U_J^a, \quad T_J^{(p)}(\xi_M) = \sum_{a=1}^{3} \varphi_a^{(p)}(\xi_M) T_J^a, \tag{53}$$

where $\varphi_M^{(p)}(\xi_M)$ is the pth derivative of the shape function with respect to ξ_M.

The generalized displacement contribution (U_I) from the single boundary element Γ consists of two parts: the generalized boundary displacement (U_I^U) and traction (U_I^T) contributions, which are added. For the straight element with the quadratic interpolation, each contribution can be evaluated analytically as given by

$$\begin{aligned} U_I^T(z) &= \sum_{a=1}^{3} \sum_{J=1}^{4} U_{IJ}^{Ta}(z)\, T_J^a, \\ U_I^U(z) &= \sum_{a=1}^{3} \sum_{J=1}^{4} U_{IJ}^{Ua}(z)\, U_J^a, \end{aligned} \tag{54}$$

with

$$U_{IJ}^{Ta}(z) = 2\Re\left\{\frac{1}{2\pi i}\sum_{M=1}^{4} A_{IM}A_{JM}\mathscr{U}_M^{Ta}(z_M)\right\},$$
$$U_{IJ}^{Ua}(z) = 2\Re\left\{\frac{1}{2\pi i}\sum_{M=1}^{4} A_{IM}L_{JM}\mathscr{U}_M^{Ua}(z_M)\right\}, \tag{55}$$

and

$$\mathscr{U}_M^{Ta}(z_M) = \frac{1}{\cos\phi + p_M\sin\phi}\sum_{d=1}^{3}(-1)^{d-1}\left[\varphi_a^{(d-1)}(\xi_M)\ln^{[d]}(z_M-\xi_M)\right]_{\xi_M^1}^{\xi_M^2},$$
$$\mathscr{U}_M^{Ua}(z_M) = \sum_{d=0}^{2}(-1)^{d}\left[\varphi_a^{(d)}(\xi_M)\ln^{[d]}(z_M-\xi_M)\right]_{\xi_M^1}^{\xi_M^2}, \tag{56}$$

where ϕ is the slope of the element Γ and $\ln^{[d]}(z_M-\xi_M)$ is the dth integral of $\ln(z_M-\xi_M)$ with respect to the argument ξ_M and is given by

$$\ln^{[d]}(z_M-\xi_M) = (-1)^d\frac{1}{d!}(z_M-\xi_M)^d\left\{\ln(z_M-\xi_M) - \sum_{j=1}^{d}\frac{1}{j}\right\} \quad (d\geqslant 0). \tag{57}$$

When d is a negative integer $\ln^{[d]}(z_M-\xi_M)$ is interpreted as the derivative instead of the integral so that

$$\ln^{[-1]}(z_M-\xi_M) = -\frac{1}{z_M-\xi_M}, \quad \ln^{[-2]}(z_M-\xi_M) = -\frac{1}{(z_M-\xi_M)^2}. \tag{58}$$

Let image of Γ in the ξ_M plane be Γ_M; we select the branch cut for $\ln(z_M-\xi_M)$ to be a straight line emanating from ξ_M (the branch point) and extending indefinitely toward ξ_M^1 (the first end point of Γ_M).

4.2. Dynamic regular boundary element

The DRBEM uses the same discretization scheme as the SSBEM: linear element and quadratic interpolation, except we use the quadratic shape functions of the arc length variable $0\leqslant l\leqslant L$ given by

$$\psi_1(l) = \frac{2}{L^2}\left(l-\frac{L}{2}\right)(l-L), \quad \psi_2(l) = \frac{2}{L^2}\left(l-\frac{L}{2}\right)l, \quad \psi_3(l) = -\frac{4}{L^2}l(l-L) \tag{59}$$

and their dth derivatives $\psi_a^{(d)}(l)$ with respect to l.

Denote the integral along the unit circle for the fundamental solutions as **n**-integral and the boundary integrals of the Somigliana's identity (10) as l-integral. The substitution of (dynamic regular part of) the fundamental generalized displacement and traction solutions, (31) and (36), into (10) results in a double integral representation of Somigliana's identity

$$U_K^{\mathrm{R}}(\mathbf{x},\omega) = \int_{\partial A} T_J(\mathbf{y},\omega)\left\{\int_{|\mathbf{n}|=1}\overline{G}_{JK}^{\mathrm{R}}(\mathbf{n}\cdot(\mathbf{y}-\mathbf{x}),\mathbf{n})\mathrm{d}\mathbf{n}\right\}\mathrm{d}l(\mathbf{y})$$
$$-\int_{\partial A} U_J(\mathbf{y},\omega)\left\{\int_{|\mathbf{n}|=1}\overline{H}_{JK}^{\mathrm{R}}(\mathbf{n}\cdot(\mathbf{y}-\mathbf{x}),\mathbf{n};\mathbf{v})\mathrm{d}\mathbf{n}\right\}\mathrm{d}l(\mathbf{y}). \tag{60}$$

Swap the order of integration in (60) to get

$$U_K^{\mathrm{R}}(\mathbf{x},\omega)=\int_{|\mathbf{n}|=1}\left\{\int_{\partial A}T_J(\mathbf{y},\omega)\overline{G}_{JK}^{\mathrm{R}}(\mathbf{n}\cdot(\mathbf{y}-\mathbf{x}),\mathbf{n})dl(\mathbf{y})\right\}\mathrm{d}\mathbf{n}$$
$$-\int_{|\mathbf{n}|=1}\left\{\int_{\partial A}U_J(\mathbf{y},\omega)\overline{H}_{JK}^{\mathrm{R}}(\mathbf{n}\cdot(\mathbf{y}-\mathbf{x}),\mathbf{n};\mathbf{v})\mathrm{d}l(\mathbf{y})\right\}\mathrm{d}\mathbf{n}. \tag{61}$$

Approximate the boundary ∂A in (61) with straight boundary elements and consider two l-integrals over an element Γ

$$\begin{aligned}\overline{I}_K(\mathbf{x}\cdot\mathbf{n},\mathbf{n},\omega)&=\int_{\Gamma}T_J(\mathbf{y},\omega)\overline{G}_{JK}^{\mathrm{R}}(\mathbf{n}\cdot(\mathbf{y}-\mathbf{x}),\mathbf{n})\mathrm{d}l(\mathbf{y}),\\ \bar{J}_K(\mathbf{x}\cdot\mathbf{n},\mathbf{n},\omega)&=\int_{\Gamma}U_J(\mathbf{y},\omega)\overline{H}_{JK}^{\mathrm{R}}(\mathbf{n}\cdot(\mathbf{y}-\mathbf{x}),\mathbf{n};\mathbf{v})\mathrm{d}l(\mathbf{y}).\end{aligned} \tag{62}$$

Analytical evaluation of these integrals is given by

$$\begin{aligned}\overline{I}_K(\mathbf{x}\cdot\mathbf{n},\mathbf{n},\omega)&=\sum_{a=1}^{3}\sum_{J=1}^{4}\overline{\mathbf{I}}_{JK}^{a}(\mathbf{x}\cdot\mathbf{n},\mathbf{n},\omega)T_J^a,\\ \overline{J}_K(\mathbf{x}\cdot\mathbf{n},\mathbf{n},\omega)&=\sum_{a=1}^{3}\sum_{J=1}^{4}\overline{\mathbf{J}}_{JK}^{a}(\mathbf{x}\cdot\mathbf{n},\mathbf{n},\omega)U_J^a,\end{aligned} \tag{63}$$

with

$$\begin{aligned}\overline{\mathbf{I}}_{JK}^{a}(\mathbf{x}\cdot\mathbf{n},\mathbf{n},\omega)&=\frac{1}{8\pi^2}\sum_{m=1}^{3}\frac{1}{\rho c_m^2}\frac{\mathscr{E}_{JK}^{m}}{E_{qq}^{m}}\mathscr{I}_a^m(\mathbf{x}\cdot\mathbf{n},\mathbf{n},\omega),\\ \overline{\mathbf{J}}_{JK}^{a}(\mathbf{x}\cdot\mathbf{n},\mathbf{n},\omega)&=\frac{1}{8\pi^2}\sum_{m=1}^{3}\frac{1}{\rho c_m^2}\frac{\mathscr{E}_{JK}^{*m}}{E_{qq}^{m}}\mathscr{J}_a^m(\mathbf{x}\cdot\mathbf{n},\mathbf{n},\omega)\end{aligned} \tag{64}$$

and

$$\begin{aligned}\mathscr{I}_a^m(\mathbf{x}\cdot\mathbf{n},\mathbf{n},\omega)&=-\sum_{d=1}^{3}\left(\frac{-1}{e_\alpha n_\alpha}\right)^d\left[\psi_a^{(d-1)}(l)\left\{\frac{\phi^{[d]}(\zeta_m)}{(k_m)^d}+2\ln^{[d]}(\zeta)\right\}\right]_{l=0}^{l=L},\\ \mathscr{J}_a^m(\mathbf{x}\cdot\mathbf{n},\mathbf{n},\omega)&=-\sum_{d=1}^{3}\left(\frac{-1}{e_\alpha n_\alpha}\right)^d\left[\psi_a^{(d-1)}(l)\left\{\frac{\phi^{[d-1]}(\zeta_m)}{(k_m)^d}+2\ln^{[d-1]}(\zeta)\right\}\right]_{l=0}^{l=L}.\end{aligned} \tag{65}$$

Here $\phi^{[d]}(\zeta_m)$ and $\ln^{[d]}(\zeta)$ are the dth integrals of $\phi(\zeta_m)$ and $\ln(\zeta)$ given by

$$\begin{aligned}\phi^{[0]}(\zeta_m)&=i\pi e^{i\zeta_m}-2[\cos(\zeta_m)\mathrm{ci}(\zeta_m)+\sin(\zeta_m)\mathrm{si}(\zeta_m)],\\ \phi^{[1]}(\zeta_m)&=\pi e^{i\zeta_m}-2[\sin(\zeta_m)\mathrm{ci}(\zeta_m)-\cos(\zeta_m)\mathrm{si}(\zeta_m)],\\ \phi^{[2]}(\zeta_m)&=-i\pi e^{i\zeta_m}+2[\cos(\zeta_m)\mathrm{ci}(\zeta_m)+\sin(\zeta_m)\mathrm{si}(\zeta_m)]-2\ln|\zeta_m|,\\ \phi^{[3]}(\zeta_m)&=-\pi e^{i\zeta_m}+2[\sin(\zeta_m)\mathrm{ci}(\zeta_m)-\cos(\zeta_m)\mathrm{si}(\zeta_m)]-2\zeta_m[\ln|\zeta_m|-1]\end{aligned} \tag{66}$$

and

$$\ln^{[d]}(\zeta)=\frac{\zeta^d}{d!}\left\{\ln|\zeta|-\sum_{j=1}^{d}\frac{1}{j}\right\}\quad(d\geqslant 0), \tag{67}$$

in terms of the arguments

Table 1
Reference values for material constants and field variables in piezoelectricity

Displacement	$u_0 = x_0\epsilon_0 = 10^{-3}x_0$ (m)	Elec. potential	$\phi_0 = x_0E_0 = 10^{7}x_0$ (V)
Stiffness	$c_0 = \dfrac{\sigma_0}{\epsilon_0} = 10^{11}$ (N/m^2)	Permittivity	$\epsilon_0 = \dfrac{D_0}{E_0} = 10^{-9}$ (C/(mV))
Compliance	$s_0 = \dfrac{\epsilon_0}{\sigma_0} = 10^{-11}$ (m^2/N)	Impermeability	$\beta_0 = \dfrac{E_0}{D_0} = 10^{9}$ (mV/C)
Piezoelectric	$e_0 = \dfrac{\sigma_0}{E_0} = 10^{1}$ (N/(mV))	Piezoelectric	$g_0 = \dfrac{E_0}{\sigma_0} = 10^{-1}$ (mV/N)
Stress constant	$= \dfrac{D_0}{\epsilon_0} = 10^{1}$ (C/m^2)	Strain constant	$= \dfrac{\epsilon_0}{D_0} = 10^{-1}$ (m^2/C)

$$\zeta_m = k_m\zeta, \quad \zeta = n_\beta(y_\beta - x_\beta) = n_\beta\{(y_\beta|_{l=0} + le_\beta) - x_\beta\}, \tag{68}$$

where e_β is the unit vector along the boundary element Γ.

The generalized displacement contribution from a single boundary element is finally given in a form

$$u_K^{\mathrm{R}}(\mathbf{x},\omega) = \int_{|\mathbf{n}|=1} \overline{I}_K(\mathbf{x}\cdot\mathbf{n},\mathbf{n},\omega)\mathrm{d}\mathbf{n} - \int_{|\mathbf{n}|=1} \overline{J}_K(\mathbf{x}\cdot\mathbf{n},\mathbf{n},\omega)\mathrm{d}\mathbf{n}, \tag{69}$$

involving single integrals over a unit circle, which can be reduced to a half-circle integration exploiting a two-fold symmetry of the integrands. A remarkable advantage of the proposed time-harmonic boundary element is that the burden of numerical integration remains comparable to that for the standard static BEM involving quadrature integration over the element.

4.3. Normalization

The order of magnitudes of the material constants and the corresponding field variables in piezoelectricity has a wide spectrum. For example, the elastic stiffness, the piezoelectric stress and the dielectric permittivity constants are of the order of 10^{11} (N/m^2), 10^{1} (C/m^2) and 10^{-9} (C/(mV)), respectively, and the strain and the electric fields are of the order of 10^{-3} and 10^{7} (V/m), respectively. The normalization of these constants and variables is essential to avoid truncation errors. Let q and q_0 represent a dimensional quantity and its reference value, respectively; its normalization is given by $\bar{q} = q/q_0$. We select the reference values for the stress, strain, electric induction, and the electric fields to be $\sigma_0 = 10^8$ (N/m^2), $\epsilon_0 = 10^{-3}$, $D_0 = 10^{-2}$ (C/m^2), and $E_0 = 10^7$ (V/m), respectively. Also select the reference value of the phase velocity to be $v_0 = 10^4$ (m/sec). The reference values of other quantities are determined in terms of these five reference variables such that the normalized governing equations remain exactly the same form as the original equations. For example, the reference value of the density is given by $\rho_0 = 10^3$ (kg/m^3). Table 1 lists other reference values for the material constants and field variables in piezoelectricity used in this paper, where x_0 (m) is the characteristic length of the problem.

5. Eigenvalue analysis

5.1. Controlling parameter in eigenvalue analysis

As seen from (34), the fundamental solutions depend on a non-dimensional parameter

$$\kappa_m = k_m r, \tag{70}$$

where $r = |\mathbf{y} - \mathbf{x}|$ and $k_m (m = 1,2,3)$ is the wave number defined by (23). Let $\bar{k}_m, \bar{v}_m$ and $\bar{r}$ be the normalized wave number, phase velocity and distance, respectively, defined by

$$\bar{k}_m = x_0 k_m, \quad \bar{v}_m = \frac{v_m}{v_0}, \quad \bar{r} = \frac{r}{x_0}. \tag{71}$$

We can rewrite (70) as

$$\kappa_m = k_m r = \bar{k}_m \bar{r}, \tag{72}$$

where

$$\bar{k}_m = \frac{\bar{\omega}}{\bar{v}_m} \tag{73}$$

is the normalized wave number which, along with $\bar{v}_m$, varies over the unit circle $|\mathbf{n}| = 1$. Since the value of $\bar{v}_m$ is of the order of 1, we can replace (73) by

$$\bar{k}_m \sim \bar{\omega} \tag{74}$$

so that (72) is given by

$$\kappa_m \sim \bar{\omega}\bar{r} \tag{75}$$

for $m = 1,2,3$. Thus we use $\bar{\omega}$ as the controlling parameter in the eigenvalue analysis. The actual radial frequency is given by

$$\omega = \frac{v_0}{x_0}\bar{\omega}. \tag{76}$$

5.2. Basic equations

The direct formulation relates the generalized boundary displacement ($\{\overline{\mathbf{U}}\}$) and traction ($\{\overline{\mathbf{T}}\}$) by a system of boundary integral equations

$$[\mathbf{H}(\bar{\omega})]\{\overline{\mathbf{U}}\} - [\mathbf{G}(\bar{\omega})]\{\overline{\mathbf{T}}\} = \{\mathbf{0}\}, \tag{77}$$

where $[\mathbf{H}(\bar{\omega})]$ and $[\mathbf{G}(\bar{\omega})]$ are square matrices of dimension N. Given a homogeneous boundary condition we select a vector $\{\overline{\mathbf{R}}\}$ of dimension N consisting of nonzero components of the boundary quantities; it may consists entirely of the generalized displacement or traction components or a mixture of both. Rearrange the columns of $[\mathbf{H}(\bar{\omega})]$ and $[\mathbf{G}(\bar{\omega})]$ that correspond to the nonzero components into a single square matrix $[\mathbf{Q}(\bar{\omega})]$ of dimension N to get the updated system of boundary integral equations

$$[\mathbf{Q}(\bar{\omega})]\{\overline{\mathbf{R}}\} = \{\mathbf{0}\}. \tag{78}$$

The matrix $[\mathbf{Q}(\bar{\omega})]$ is complex valued, nonsymmetric and its components are non-linear functions of the angular frequency $\bar{\omega}$. Determination of pairs of $\bar{\omega}$ (eigenvalue) and nonzero $\{\overline{\mathbf{R}}\}$ (eigen vector) is the goal of the eigenvalue analysis. The direct search method (Kitahara, 1985) calculates $\det[\mathbf{Q}(\bar{\omega})]$ at multiple sequential values of $\bar{\omega}$ in a given interval. The accuracy of this method is strongly influenced by the increment size $\Delta\bar{\omega}$. The true zero points of the determinant are never achieved numerically; instead, eigen frequencies obtained correspond to the local minima. Furthermore, the direct search method has a difficulty in computing multiple or clustered eigenvalues.

We approximate $[\mathbf{Q}(\bar{\omega})]$ in a given interval $[\bar{\omega}_A, \bar{\omega}_B]$ by a matrix polynomial of order M; the approximate eigenvalue problem is given by

$$[[\mathbf{Q}_0] + \bar{\omega}[\mathbf{Q}_1] + \bar{\omega}^2[\mathbf{Q}_2] + \cdots + \bar{\omega}^M[\mathbf{Q}_M]]\{\overline{\mathbf{R}}\} = \{\mathbf{0}\}, \tag{79}$$

where $[\mathbf{Q}_0], [\mathbf{Q}_1], \ldots, [\mathbf{Q}_M]$ are square coefficient matrices of dimension N determined by Newton's divided differences. Introduce a series of vectors, $\{\overline{\mathbf{R}}_i\} = \bar{\omega}^i\{\overline{\mathbf{R}}\}$ $(i = 0, 1, \ldots, M)$, to rewrite (79) as

$$[\mathbf{Q}_0]\{\overline{\mathbf{R}}_0\} + [\mathbf{Q}_1]\{\overline{\mathbf{R}}_1\} + [\mathbf{Q}_2]\{\overline{\mathbf{R}}_2\} + \cdots + [\mathbf{Q}_M]\{\overline{\mathbf{R}}_M\} = \{\mathbf{0}\}. \tag{80}$$

Eq. (80) is equivalent to a linear general eigenvalue problem

$$[\mathbf{Q}^*]\{\overline{\mathbf{R}}^*\} = \bar{\omega}[\mathbf{P}^*]\{\overline{\mathbf{R}}^*\}, \tag{81}$$

where $[\mathbf{Q}^*]$ and $[\mathbf{P}^*]$ are square matrices of dimension MN and $\{\overline{\mathbf{R}}^*\}$ is a vector of dimension MN defined by

$$[\mathbf{Q}^*] = \begin{bmatrix} [\mathbf{Q}_{M-1}] & [\mathbf{Q}_{M-2}] & \cdots & [\mathbf{Q}_2] & [\mathbf{Q}_1] & [\mathbf{Q}_0] \\ [\mathbf{I}] & [\mathbf{0}] & \cdots & [\mathbf{0}] & [\mathbf{0}] & [\mathbf{0}] \\ [\mathbf{0}] & [\mathbf{I}] & \cdots & [\mathbf{0}] & [\mathbf{0}] & [\mathbf{0}] \\ \cdots & \cdots & \cdots & \cdots & \cdots & \cdots \\ [\mathbf{0}] & [\mathbf{0}] & \cdots & [\mathbf{I}] & [\mathbf{0}] & [\mathbf{0}] \\ [\mathbf{0}] & [\mathbf{0}] & \cdots & [\mathbf{0}] & [\mathbf{I}] & [\mathbf{0}] \end{bmatrix}, \quad [\mathbf{P}^*] = \begin{bmatrix} -[\mathbf{Q}_M] & [\mathbf{0}] & [\mathbf{0}] & \cdots & [\mathbf{0}] & [\mathbf{0}] \\ [\mathbf{0}] & [\mathbf{I}] & [\mathbf{0}] & \cdots & [\mathbf{0}] & [\mathbf{0}] \\ [\mathbf{0}] & [\mathbf{0}] & [\mathbf{I}] & \cdots & [\mathbf{0}] & [\mathbf{0}] \\ \cdots & \cdots & \cdots & \cdots & \cdots & \cdots \\ [\mathbf{0}] & [\mathbf{0}] & [\mathbf{0}] & \cdots & [\mathbf{I}] & [\mathbf{0}] \\ [\mathbf{0}] & [\mathbf{0}] & [\mathbf{0}] & \cdots & [\mathbf{0}] & [\mathbf{I}] \end{bmatrix},$$

$$[\overline{\mathbf{R}}^*] = \begin{Bmatrix} \bar{\omega}^{M-1}\{\overline{\mathbf{R}}\} \\ \bar{\omega}^{M-2}\{\overline{\mathbf{R}}\} \\ \bar{\omega}^{M-3}\{\overline{\mathbf{R}}\} \\ \cdots \\ \bar{\omega}\{\overline{\mathbf{R}}\} \\ \{\overline{\mathbf{R}}\} \end{Bmatrix}, \tag{82}$$

where $[\mathbf{I}]$ and $[\mathbf{0}]$ are the identity and zero matrices of dimension N.

5.3. Eigen solvers

5.3.1. QZ algorithm

For solids of general anisotropy, Denda et al. (2003) have reduced the non-linear eigenvalue problem (78) to the generalized linear eigenvalue problem (81) and solved the latter by the QZ algorithm. Let N be the number of degrees of freedom of the problem, which is four times the number of nodes in piezoelectricity. The QZ algorithm using the Mth order polynomial approximation (79) of the determinant in the interval $(\bar{\omega}_A, \bar{\omega}_B)$ deals with $NM \times NM$ square matrices $[\mathbf{Q}^*]$ and $[\mathbf{P}^*]$ in (82) to produce NM eigenvalues. While we seek for real eigenvalues in this interval, the majority of the eigenvalues are either complex valued or real but out of this interval, and they are called spurious. We look for eigenvalues $\bar{\omega}$ with small imaginary parts that satisfy the condition,

$$|\Im[\bar{\omega}]| \leqslant \epsilon_{im} \Re[\bar{\omega}], \tag{83}$$

where the $\Re$ indicates the real part of a complex variable and ϵ_{im} is the tolerance for the imaginary parts of the eigenvalues specified a priori. The rest of the eigenvalues have large imaginary parts and have to be rejected as spurious. Even among those with small imaginary parts, some still have to be rejected as spurious if their real parts are outside the sub-interval $(\bar{\omega}_A, \bar{\omega}_B)$. These eigenvalues belong to the adjacent sub-intervals, where their values are determined more accurately than in the current sub-interval. This brings up the second condition

$$\bar{\omega}_A \leqslant \Re[\bar{\omega}] \leqslant \bar{\omega}_B \tag{84}$$

for the selection of the eigenvalues. Although a higher value of M in (79) allows a larger interval of $\bar{\omega}$ containing more eigenvalues, it inflates the size of $\mathbf{Q}^*$. A better strategy is to use a low value such as $M = 1$ for a small interval containing a small number of eigenvalues. The latter strategy requires more intervals, but computation for each interval is much faster than the former due to the small size of the matrices. Even

with this better strategy, the typical ratio of non-spurious to spurious eigenvalues is 1 to N, which is an enormous waste despite the high accuracy of the algorithm.

5.3.2. IRAM

The implicitly restarted Arnoldi method (IRAM) (Lehoucq et al., 1998) eliminates this waste and provides an accurate and dramatically faster eigen solver than the QZ algorithm. We select $M = 1$ in (79) to give the linear approximation of (78) in $\bar{\omega} \in (\bar{\omega}_A, \bar{\omega}_B)$. This sets the generalized eigenvalue problem,

$$[\mathbf{A}]\{\overline{\mathbf{R}}\} = \bar{\omega}[\mathbf{B}]\{\overline{\mathbf{R}}\}, \tag{85}$$

where $[\mathbf{A}] = [\mathbf{Q}_0]$ and $[\mathbf{B}] = -[\mathbf{Q}_1]$. With the IRAM, we seek the real valued eigenvalues of (85) in the interval $[\bar{\omega}_A, \bar{\omega}_B]$. Besides matrices $[\mathbf{A}]$ and $[\mathbf{B}]$, the IRAM input consists of (a) real numbers $\bar{\omega}_A$ and $\bar{\omega}_B$, (b) the number k of eigenvalues in this interval, and (c) a small tolerance limit ϵ_{im} for the imaginary part of the eigenvalues. This is a variation of the standard IRAM input that consists of a complex number τ and k; the IRAM will find k eigenvalues closest to τ. We apply the shift and invert spectrum transformation to convert (85) to the standard eigenvalue problem

$$[\mathbf{C}]\{\overline{\mathbf{R}}\} = \bar{\mu}\{\overline{\mathbf{R}}\}, \tag{86}$$

where

$$[\mathbf{C}] = ([\mathbf{A}] - \bar{\tau}[\mathbf{B}])^{-1}[\mathbf{B}], \quad \bar{\mu} = \frac{1}{\bar{\omega} - \bar{\tau}} \tag{87}$$

and

$$\bar{\tau} = \frac{\bar{\omega}_A + \bar{\omega}_B}{2}. \tag{88}$$

To find the k eigenvalues $\bar{\omega}_i$ $(i = 1, \ldots, k)$ near $\bar{\tau}$ the IRAM obtains the eigenvalues $\bar{\mu}_i$ of the standard eigenvalue problem with k largest magnitudes and convert them to $\bar{\omega}_i$ using the relation

$$\bar{\omega}_i = \bar{\tau} + \frac{1}{\bar{\mu}_i}. \tag{89}$$

In general the resulting eigenvalues are complex valued and we select eigenvalues that satisfy conditions (83) and (84). The IRAM is designed to compute the specified number (i.e., k) of eigenvalues. Since the actual number of eigenvalues in the given interval is unknown, there is a chance to underestimate this number. A crude but reliable way to resolve this problem is to start solving the eigenvalue problems with an initial guess of $k = k_0$ and continue to double the number k until

$$\max_{i=1,\ldots,k} |\bar{\omega}_i - \bar{\tau}| > \frac{\Delta\bar{\omega}}{2} \tag{90}$$

is satisfied, where $\Delta\bar{\omega} = \bar{\omega}_B - \bar{\omega}_A$.

5.4. Numerical results

We have analyzed a square domain for quartz using a homogeneous mesh with 24 elements and 48 nodes. The quartz belongs to the symmetry class of Trigonal 32. Its stiffness constants are $c_{11} = 8.674$, $c_{33} = 10.72$, $c_{44} = 5.794$, $c_{12} = 0.699$, $c_{13} = 1.191$, $c_{14} = -1.791$, in the unit of 10^{10} N/m^2. The piezoelectric stress constants are $e_{x1} = 0.171$, $e_{x4} = -0.0436$, in the unit of C/m^2. The relative permittivity constants in constant strain are $\epsilon_{xx}/\epsilon_0 = 4.5$, $\epsilon_{zz}/\epsilon_0 = 4.6$, where $\epsilon_0 = 8.854 \times 10^{-12}$ farads/m. The search range considered is $0.0 \leqslant \bar{\omega} \leqslant 6.0$. Exploiting the double symmetry of the integrands, the numerical integration (69) is performed over the half-circle, which is divided into nine sub-intervals, with eight points Gauss quadrature

in each sub-interval. The number n of sub-division for the half-circle is determined to accommodate the oscillatory behavior of the integrands properly. Denda et al. (2003) has set up the guideline

$$n = \kappa_m, \tag{91}$$

which is obtained by setting the sub-interval size to be the smallest half-wave length of the oscillation. They have also performed an extensive study to establish the optimum number of Gauss quadrature points as the function of the parameter κ_m using the case study on the isotropic anti-plane strain solution. Table 2 shows the optimum number of Gauss quadrature points for the integration of the fundamental solution to achieve relative error of the order of 10^{-7}. Table 2 is also used for the guideline of integration of the boundary element coefficients. We have used the same number of Gauss points for the real and imaginary parts of the boundary element, which is slightly more conservative than the guideline set by Table 2.

We have divided the frequency range of $0.0 \leqslant \bar{\omega} \leqslant 6.0$ into sub-ranges of size $\Delta\bar{\omega} = 0.05$ and applied the QZ-algorithm with $M = 1$ and IRAM in each sub-range. For both methods, the criterion used to pick up true eigen values among spurious eigenvalues is: (a) real part is in the search region and (b) the absolute value of the imaginary part is less than 0.1, i.e., $\epsilon_{im} = 0.1$ in (86). Tables 3 and 4 list eigenvalues found for the generalized displacement and traction zero BCs along with the FEM results. The FEM has used 25 36-nodes elements; the total number of nodes for the FEM calculation is 676. The FEM 36-nodes element has 20 and 16 nodes on and inside the boundary, respectively; it covers the element uniformly by a 6×6 array of nodes. The FEM developed by Wang et al. (1999) has been used successfully for industrial

Table 2
Optimum selection of the number of quadrature points p (for imaginary part) and q (for real part) of the Radon transformed fundamental solution

	Opt. # of quad. pts.	
	p	q
$0 \leqslant \kappa_m \leqslant 10$	5	7
$0 \leqslant \kappa_m \leqslant 20$	4	6
$20 \leqslant \kappa_m \leqslant 60$	4	5

Table 3
Eigen frequencies $\bar{\omega}$ for a square quartz domain with the generalized displacement zero BC

BEM-QZ	BEM-IRAM	FEM	BEM-QZ	BEM-IRAM	FEM
2.0529163	2.0529163	2.0514446	4.4816256	4.4816256	4.4810207
2.1189051	2.1189051	2.1180479	4.5827853	4.5827853	4.5822244
2.1498585	2.1498585	2.1483615	4.9072713	4.9072713	4.9069360
2.7197398	2.7197398	2.7190529	5.0008150	5.0008150	5.0006463
2.9091266	2.9091266	2.9086841	5.2107294	5.2107294	5.2105290
2.9933909	2.9933909	2.9929622	5.2820195	5.2820195	5.2815447
3.5102774	3.5102774	3.5098855	5.3344032	5.3344032	5.3337498
3.5875497	3.5875497	3.5870780	5.3533056	5.3533056	5.3525324
3.6594485	3.6594485	3.6584456	5.4194479	5.4194479	5.4189722
3.7260255	3.7260255	3.7252852	5.5040931	5.5040931	5.5041806
3.8743249	3.8743249	3.8733734	5.6881460	5.6881460	5.6877681
3.9318375	3.9318375	3.9310687	5.7180436	5.7180436	5.7176508
4.1998843	4.1998843	4.1997178	5.7355393	5.7355393	5.7348085
4.3665248	4.3665248	4.3657533	5.7823143	5.7823143	5.7819670
4.4397478	4.4397478	4.4390138	5.9562269	5.9562269	5.9555229
4.5041277	4.5041277	4.5040515			

Table 4
Eigen frequencies $\bar{\omega}$ for a square quartz domain with the generalized traction zero BC

BEM-QZ	BEM-IRAM	FEM	BEM-QZ	BEM-IRAM	FEM
1.2145088	1.2145088	1.2089318	4.0388115	4.0388115	4.0335227
1.2623694	1.2623694	1.2564972	4.1978734	4.1978734	4.1938836
1.3975235	1.3975235	1.3932688	4.2891775	4.2891775	4.2882931
1.4318070	1.4318070	1.4300950	4.2916230	4.2916230	4.2884494
1.6934463	1.6934463	1.6961658	4.4681351	4.4681351	4.4621603
1.7361775	1.7361775	1.7377406	4.5325955	4.5325955	4.5261763
1.8395258	1.8395258	1.8397334	4.6471505	4.6471505	4.6362019
1.8926617	1.8926617	1.8958074	4.6811296	4.6811296	4.6747030
2.0610223	2.0610223	2.0610462	4.6998141	4.6998141	4.6848519
2.1071104	2.1071104	2.1069953	4.7625681	4.7625681	4.7523645
2.3897206	2.3897206	2.3894016	4.9125699	4.9125699	4.9110275
2.5082646	2.5082646	2.5001538	5.0412813	5.0412813	5.0338686
2.6151741	2.6151741	2.6107793	5.0793905	5.0793905	5.0683058
2.7759226	2.7759226	2.7701186	5.1708429	5.1708429	5.1653612
2.8057726	2.8057726	2.8020482	5.2872916	5.2872916	5.2788529
2.8969799	2.8969799	2.8936377	5.3330519	5.3330519	5.3220680
3.0407019	3.0407019	3.0358119	5.3749176	5.3749176	5.3699159
3.1717542	3.1717542	3.1676350	5.4225762	5.4225762	5.4079553
3.2724588	3.2724588	3.2686295	5.4463162	5.4463162	5.4389057
3.3188196	3.3188196	3.3192521	5.5411958	5.5411958	5.5381640
3.5145123	3.5145123	3.5116109	5.5535319	5.5535319	5.5440511
3.6335017	3.6335017	3.6272374	5.5680067	5.5680067	5.5618751
3.7235163	3.7235163	3.7236162	5.6580242	5.6580242	5.6591871
3.7326404	3.7326404	3.7322540	5.6843472	5.6843472	5.6726727
3.7726525	3.7726525	3.7751680	5.7623050	5.7623050	5.7609424
3.8056663	3.8056663	3.7996832	5.8112034	5.8112034	5.8017309
3.8087235	3.8087235	3.8130757	5.8777669	5.8777669	5.8743026
3.9955690	3.9955690	3.9843044	5.9436785	5.9436785	5.9164630
4.0283721	4.0283721	4.0203054	5.9829256	5.9829256	5.9633065

applications primarily in the frequency range $\bar{\omega} < 1$. In the frequency range $0.0 \leqslant \bar{\omega} \leqslant 6.0$ the BEM and FEM results agree up to 3 digits for displacement and traction zero BCs. The accuracy of the FEM tends to deteriorate in the high frequency range as reported by Denda et al. (2003) for the general anisotropic solids. As more higher frequency applications appear, such as the SAW using diamond, the importance of the higher frequency capability of the BEM should stand out. the The typical CPU times for QZ-algorithm and the IRAM on a PC with a 1 GHz processor are 95.8 and 11.5 s to obtain eigenvalues in one sub-interval; the time to calculate the boundary element coefficients is not included. Notice that the results by QZ-algorithm and IRAM perfectly agree up to 8 significant digits (and more) and that the IRAM is approximately 10 times faster than the QZ-algorithm. In general the time is dependent on many factors other than the algorithm such as the OS, compiler, and the optimization option.

6. Convergence study

6.1. Modified IRAM

Although the eigenvalues calculated in Section 5 were in agreement with the most reliable FEM results up to a few to several significant digits, further study on the effects of the sub-interval size $\Delta\bar{\omega}$ and the number N of the boundary elements upon the threshold size ϵ_{im} for the acceptable imaginary parts for the true

eigenvalues is needed. To examine the effects, we will catalogue the imaginary parts of the true eigenvalues obtained numerically as we change the sub-interval size $\Delta\omega$ and the number N of the boundary elements. We call this as the convergence study of the imaginary parts of the true eigenvalues. Note that, when we compute the eigen frequencies without the help of the FEM, it is difficult to get reliable results without performing the convergence study.

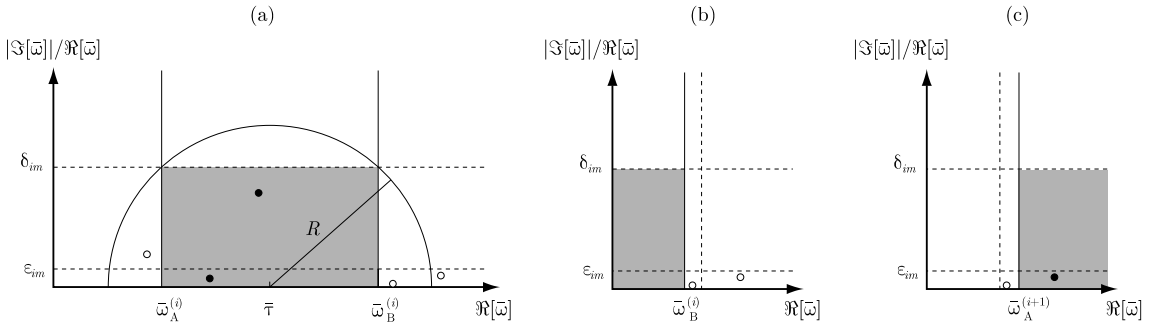

Fig. 1. (a) Selection of eigenvalues on a complex plane for the ith sub-interval. The gray rectangle indicates the region specified by (84) and (92). The black and white circles indicate the accepted and rejected eigenvalues. (b) The right boundary for the ith sub-interval. (c) The left boundary for the $i+1$th sub-interval.

Table 5
Real and imaginary parts of the eigenvalues for the square domain model computed with $N_E = 64,\ \Delta\bar{\omega} = 0.1,\ M = 1$, and $\delta_{im} = 0.05$

$\Re[\lambda]$	$\Im[\lambda]$	$\Re[\lambda]$	$\Im[\lambda]$	$\Re[\lambda]$	$\Im[\lambda]$	$\Re[\lambda]$	$\Im[\lambda]$
2.05292	2.830e−3	5.68830	1.071e−3	7.53536	2.543e−3	9.05154	2.947e−3
2.11892	1.618e−3	5.71820	1.379e−3	7.60088	9.277e−5	9.06752	2.406e−3
2.14986	2.494e−3	5.73560	1.972e−3	7.65282	2.282e−3	9.07451	2.470e−3
2.71975	2.038e−3	5.78261	1.567e−3	7.71703	1.252e−3	9.12078	1.623e−3
2.90915	9.513e−4	5.95643	2.695e−3	7.72733	2.056e−3	9.13638	2.689e−3
2.99341	7.106e−4	6.09086	1.087e−3	7.77308	2.400e−3	9.18816	1.148e−3
3.51031	9.345e−4	6.10139	1.456e−4	7.86306	2.294e−3	9.36192	2.573e−3
3.58758	1.482e−3	6.16991	2.120e−3	7.92221	1.815e−3	9.37778	1.874e−3
3.65947	3.051e−3	6.22949	2.293e−3	7.92962	2.172e−3	9.39464	5.572e−4
3.72604	1.725e−3	6.37199	2.382e−3	8.04843	2.756e−3	9.48977	1.050e−3
3.87435	2.094e−3	6.39276	6.008e−4	8.08537	1.338e−3	9.49117	7.843e−4
3.93186	1.966e−3	6.48008	1.818e−3	8.11265	1.407e−3	9.50921	1.236e−3
4.19992	8.162e−6	6.48027	2.270e−3	8.25626	2.560e−3	9.52905	1.983e−3
4.36661	2.079e−3	6.59655	3.400e−4	8.29071	1.074e−3	9.55904	2.396e−3
4.43984	2.540e−3	6.86556	2.690e−3	8.33414	2.491e−3	9.60967	7.986e−4
4.48169	1.844e−3	6.88634	1.448e−3	8.34673	2.706e−3	9.69842	1.742e−4
4.50420	5.506e−4	6.90337	3.183e−4	8.47931	1.545e−3	9.76343	2.173e−3
4.58285	1.821e−3	6.91427	1.472e−3	8.49230	1.042e−3	9.79095	9.040e−4
4.90737	6.703e−4	6.94453	2.522e−3	8.56703	2.287e−3	9.79107	7.539e−4
5.00089	9.265e−5	7.04648	2.475e−3	8.59440	6.025e−4	9.85253	2.644e−3
5.21084	1.048e−3	7.08791	1.201e−3	8.60539	5.057e−4	9.90965	1.014e−3
5.28213	1.816e−3	7.28115	1.394e−3	8.63658	2.631e−3	9.92088	2.007e−3
5.33454	2.833e−3	7.29578	4.648e−4	8.75728	2.566e−3	9.92699	2.218e−3
5.35337	2.547e−3	7.35237	3.038e−3	8.86159	2.453e−3	9.99634	3.537e−4
5.41957	1.531e−3	7.38493	1.243e−3	8.95640	2.549e−3		
5.50425	5.829e−4	7.48706	1.682e−3	8.99250	6.750e−4		

Table 6
Real and imaginary parts of the eigenvalues for the rectangular domain model computed with $N_E = 64$, $\Delta\bar{\omega} = 0.01$, $M = 1$, and $\delta_{im} = 0.05$

$\Re[\lambda]$	$\lvert \Im[\lambda] \rvert$	$\Re[\lambda]$	$\lvert \Im[\lambda] \rvert$	$\Re[\lambda]$	$\lvert \Im[\lambda] \rvert$	$\Re[\lambda]$	$\lvert \Im[\lambda] \rvert$
0.61837	4.314e−5	0.93175	6.137e−5	1.09844	8.357e−5	1.29186	6.986e−5
0.62311	6.298e−5	0.93982	9.309e−6	1.09915	1.950e−5	1.30131	7.523e−3
0.63635	6.711e−5	0.94224	3.832e−5	1.10734	7.066e−5	1.30156	1.202e−4
0.65153	3.824e−5	0.94363	4.332e−5	1.12087	2.070e−5	1.31410	1.519e−4
0.67174	4.570e−5	0.94777	3.775e−5	1.13539	7.890e−5	1.31765	2.245e−4
0.68062	2.177e−5	0.94997	2.555e−6	1.14148	8.147e−5	1.32577	2.645e−4
0.68288	5.608e−5	0.95493	4.841e−5	1.14678	6.454e−5	1.32859	2.990e−3
0.69248	5.057e−5	0.95935	1.560e−5	1.15985	4.254e−5	1.33032	3.838e−4
0.69429	7.559e−5	0.96754	3.961e−5	1.17777	5.673e−5	1.34156	8.111e−4
0.70246	4.791e−5	0.97221	7.472e−5	1.18366	8.841e−5	1.35035	1.215e−4
0.71644	6.233e−5	0.97350	7.465e−5	1.18456	1.691e−4	1.35665	2.919e−4
0.72221	5.855e−5	0.97413	4.594e−5	1.20518	7.789e−4	1.35716	1.410e−4
0.73167	4.030e−5	0.98401	4.775e−5	1.21014	9.568e−4	1.35752	1.589e−4
0.75092	2.998e−5	0.99366	4.403e−5	1.21684	1.064e−3	1.36429	1.673e−4
0.75169	4.313e−5	1.00535	4.865e−5	1.22807	1.086e−4	1.36553	3.646e−4
0.77191	4.515e−5	1.00762	6.158e−5	1.22939	6.074e−5	1.37686	1.309e−4
0.78352	7.775e−5	1.01371	1.116e−4	1.23419	3.237e−4	1.37870	4.286e−4
0.79568	7.104e−5	1.01759	3.694e−5	1.24850	1.862e−4	1.38290	2.683e−4
0.81790	5.942e−5	1.03129	2.384e−5	1.25012	1.193e−4	1.38387	2.243e−4
0.82098	2.719e−5	1.04213	6.115e−5	1.25389	1.147e−4	1.38525	3.442e−4
0.84857	3.997e−5	1.04615	4.769e−5	1.25611	7.990e−4	1.38941	6.696e−2
0.85449	9.325e−5	1.05591	1.283e−4	1.27084	8.984e−5	1.39868	5.563e−5
0.87744	6.054e−5	1.06260	4.083e−5	1.27739	1.461e−4		
0.89226	6.894e−5	1.07587	7.635e−5	1.28155	2.719e−4		
0.90816	4.969e−5	1.07985	5.827e−6	1.28667	2.639e−3		

To perform the convergence study using the IRAM, we propose its modified version, where we select a much looser threshold value δ_{im} for the imaginary part of the complex eigenvalues than ϵ_{im} in (83). This way, we extend the search region from the sub-interval $(\bar{\omega}_A, \bar{\omega}_B)$ on the real axis to a rectangular region with the vertical extent

$$|\Im[\bar{\omega}]| \leqslant \delta_{im} \Re[\bar{\omega}]. \tag{92}$$

Also we replace the condition (90) with

$$\max_{i=1,k} |\bar{\omega}_i - \bar{\tau}| > R, \tag{93}$$

where R is the extended search radius defined by

$$R \equiv \sqrt{\left(\frac{\bar{\omega}_A + \bar{\omega}_B}{2}\right)^2 + (\delta_{im} \Re[\bar{\omega}])^2}, \tag{94}$$

which is the radius of a circle centered at the midpoint $\bar{\tau}$ of the sub-interval $[\bar{\omega}_A, \bar{\omega}_B]$. Fig. 1(a) schematically illustrates condition (93) together with conditions (92) (or (83)). The condition (93) effectively tells that all eigenvalues within the extended search radius R from the center of the interval have been picked up. Note that the threshold value δ_{im} is deliberately chosen to be much larger than ϵ_{im} to pick up eigenvalues with larger imaginary parts than used in Section 5.3.2. Such eigenvalues are necessary to examine the behavior of the imaginary parts of the eigenvalues in the current convergence study.

Another problem we have encountered in Section 5.3.2 is the possibility of missing eigenvalues that are on or very close to the boundary between two adjacent intervals. As shown in Fig. 1(b) and (c), such eigenvalues may be missed by both the current and the adjacent intervals. One way to avoid this is to move the boundary and compute the eigenvalues for the new sub-intervals all over again. Another way is to replace (84) with

$$\bar{\omega}_A - \epsilon_{\mathrm{re}} \leqslant \Re[\bar{\omega}] \leqslant \bar{\omega}_B + \epsilon_{\mathrm{re}}, \tag{95}$$

where a positive real number ϵ_{re} is the tolerance specified prior to the analysis. Although this may yield redundant eigenvalues in two adjacent sub-intervals, the redundant eigenvalues can be removed by checking the orthogonality of eigenvectors.

6.2. Numerical study on the imaginary parts of the eigenvalues

We have applied the modified IRAM Algorithm of Section 6.1 for the determination of eigen frequencies of two quartz plates: a square quartz domain and a rectangular AT-cut quartz domain with the aspect ratio 1/15. The non-dimensional eigen frequencies $\bar{\omega}$ obtained for the square plate here can be used to calculate the actual eigen frequencies of any square quartz plates of edge length x_0 by the formula $\omega = (v_0/x_0)\bar{\omega}$, where $v_0 = 10^4$ m/s is the reference phase velocity. Similarly, $\bar{\omega}$ obtained here for the rectangular AT-cut quartz plate gives the eigen frequencies of any rectangular AT-cut quartz plates with the aspect ratio 1/15 and the short edge length x_0 by the formula $\omega = 2(v_0/x_0)\bar{\omega}$.

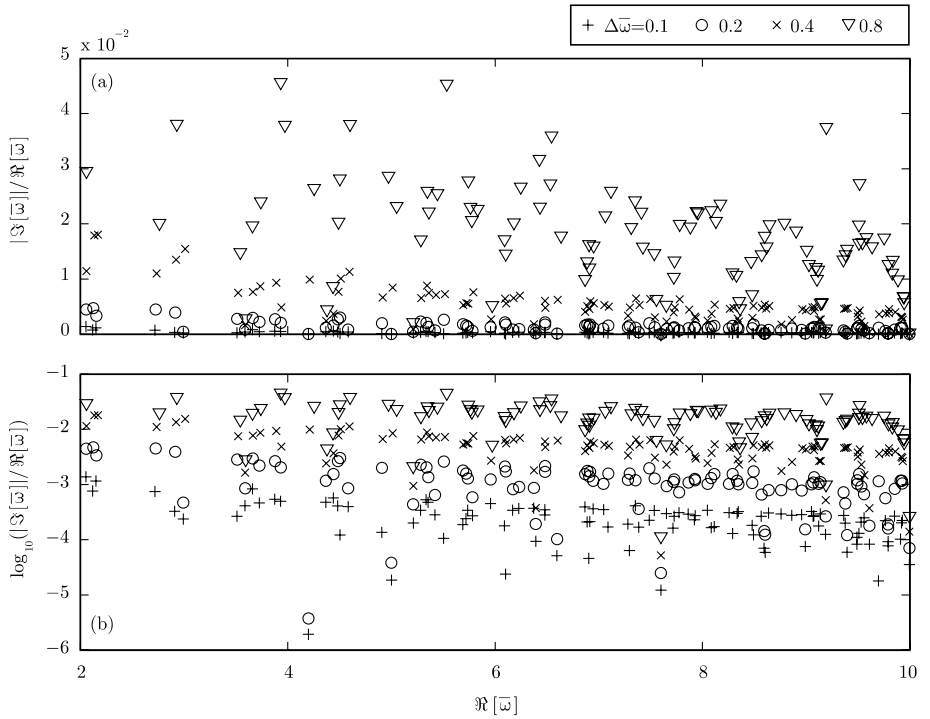

Fig. 2. Real part and normalized imaginary part of the eigenvalues for the square domain model computed with $N_E = 64$ and $\Delta\bar{\omega} = 0.1, 0.2, 0.4, 0.8$.

We have used the uniform mesh for locating boundary nodes in both plates. Let the number of boundary elements in each plate be N_E, then the number of nodes is $2N_E$ and the DOF $8N_E$. Zero generalized displacement boundary condition is considered for both plates. The ranges of the non-dimensional eigenfrequency $\bar{\omega}$ sought are $[0, 10]$ and $[0, 1.4]$ for the square and rectangular plates, respectively. We have used the linear function ($M = 1$) in the piecewise polynomial approximation. The parameters in the modified IRAM Algorithm are set as, $k_0 = 10$ and $\delta_{im} = 0.05$.

The results of the convergence study are summarized in Tables 5 and 6 and Figs. 2–5. Tables 5 and 6 enlist only the most accurate results for the square quartz ($N_E = 64$ and $\Delta\bar{\omega} = 0.1$) and rectangular AT-cut quartz ($N_E = 64$ and $\Delta\bar{\omega} = 0.01$) plates, obtained from the finest boundary element mesh and the smallest sub-interval size for each plate. The wide variation on the range of their imaginary parts observed in Figs. 2–5 are the results of allowing relatively tolerant threshold value δ_{im} for the imaginary part, which was deliberately set up for the convergence study.

Fig. 2 depicts the eigenvalues of the square quartz plate for different values of $\Delta\bar{\omega} = 0.1, 0.2, 0.4$, and 0.8 at the fixed number $N_E = 64$ of the boundary elements: the absolute values of the normalized imaginary parts of the true eigenvalues are presented by the (a) normal and (b) logarithmic plots. These plots show that the imaginary parts of the eigenvalues become small as $\Delta\bar{\omega}$ decreases at a fixed number of the boundary elements.

Fig. 3 illustrates the results of the square quartz plate by changing the number of elements ($N_E = 64$, 32, 16, and 8) at a fixed interval $\Delta\bar{\omega} = 0.1$. An interesting discovery from these plots is the phenomenon of the sudden bursts in the magnitude of the imaginary part at higher frequencies. Each burst is followed by the

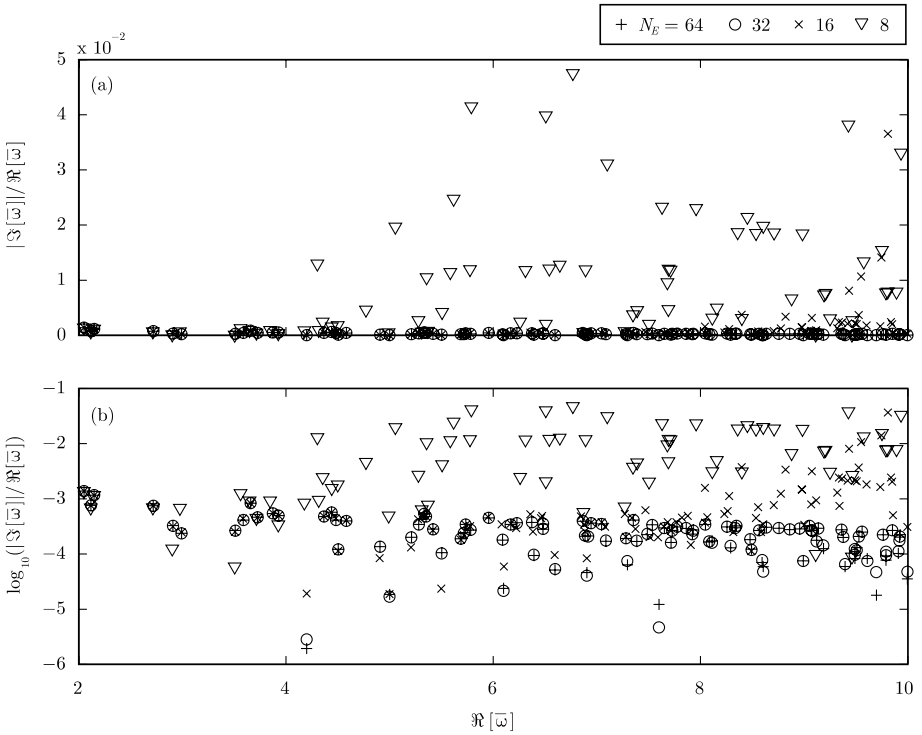

Fig. 3. Real part and normalized imaginary part of the eigenvalues for the square domain model computed with $N_E = 64,32,16,8$ and $\Delta\bar{\omega} = 0.1$.

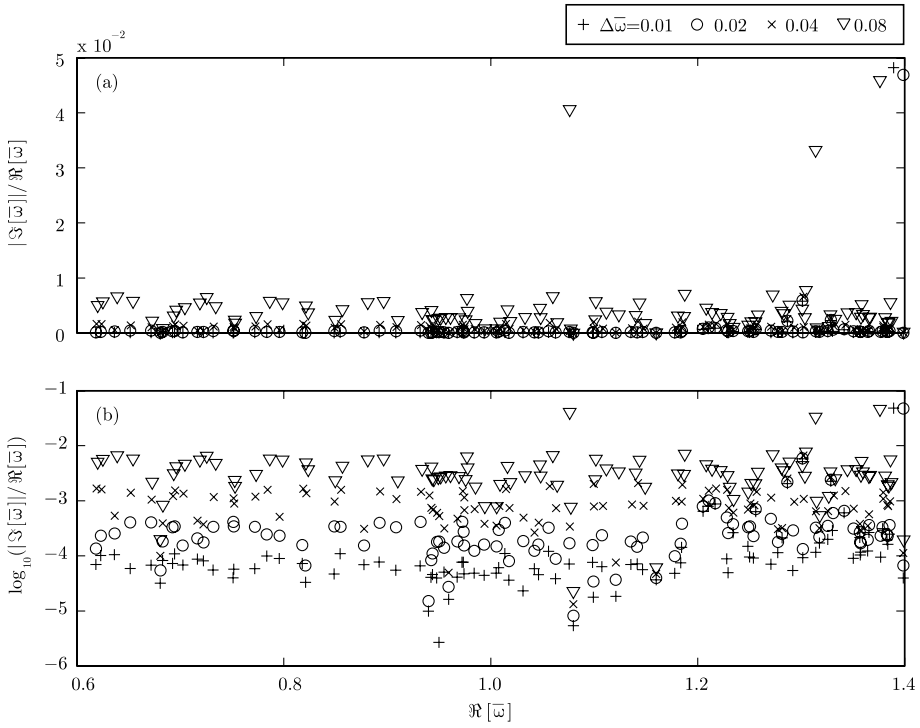

Fig. 4. Real part and normalized imaginary part of the eigenvalues for the rectangular domain model computed with $N_E = 64$ and $\Delta\bar{\omega} = 0.01, 0.02, 0.04, 0.08$.

temporal recovery back to the low value of the imaginary part. The value of the eigen frequency at the initial occurrence of this burst becomes higher as N_E increases. This suggests that observing the imaginary part provides us with the basis to determine how many boundary elements are necessary to get the eigen frequencies having required level of accuracy in the given frequency range.

The final observation is on the sensitivity of the eigenvalues. If the true eigenvalues closely clustered near the real axis are well separated from the spurious eigenvalues that have large imaginary parts, then the solution is insensitive to the value of ϵ_{im} used in (83). We observe that the eigenvalues become more sensitive to ϵ_{im} as $\Delta\omega$ increases or N decreases since the distribution of the eigenvalues under these circumstances becomes more scattered away from the real axis.

The results for the rectangular plate are shown in Figs. 4 and 5 with a fixed $N = 64$ and variable $\Delta\bar{\omega} = 0.01, 0.02$, and 0.04 and with a fixed $\Delta\bar{\omega} = 0.01$ and variable $N =$ 16, 32, and 64, respectively. The results shown in these figures confirm the observation made for the square plate results.

7. Conclusions

We have developed a time-harmonic BEM for piezoelectric solids in 2-D using the fundamental solution obtained by Radon transform. The boundary element coefficients are evaluated numerically by the single line integral over the unit circle. We have applied the BEM to the eigenvalue analysis using the QZ algorithm and the IRAM. The eigen frequency results by the two methods are virtually identical and are in

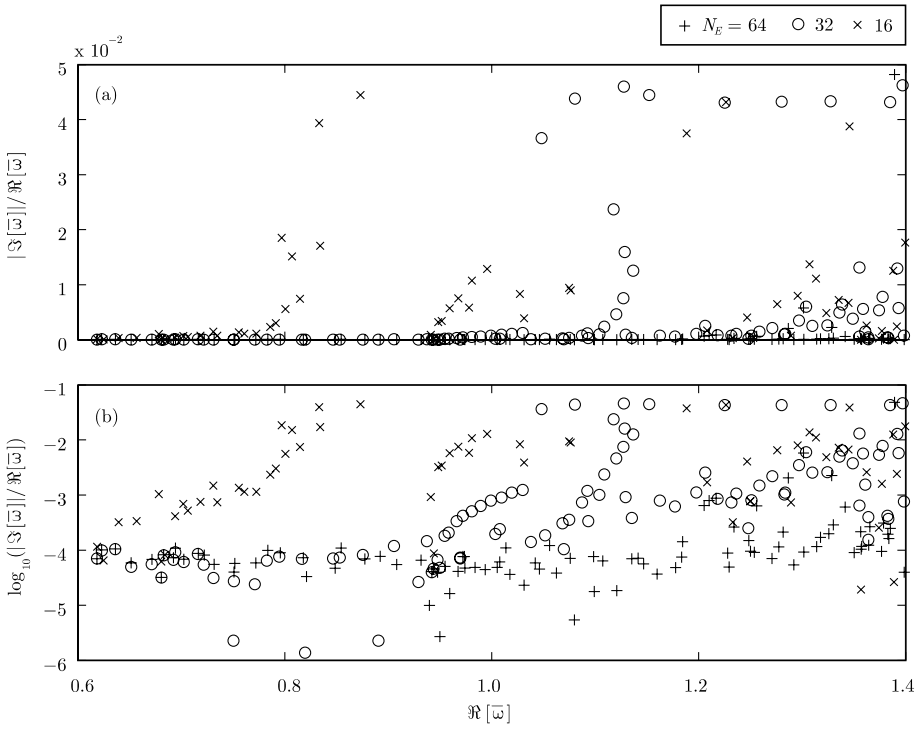

Fig. 5. Real part and normalized imaginary part of the eigenvalues for the rectangular domain model computed with $N_E = 64,32,16$ and $\Delta\bar{\omega} = 0.01$.

agreement with the FEM results up to a few significant digits. The IRAM is approximately 10 times faster than the QZ-algorithm. We have also presented a framework for the convergence study. We have examined how the values of the imaginary parts of the eigenvalues are influenced by the sub-interval size and by the number of boundary elements. We have demonstrated that observing the imaginary part of the complex eigenvalues in the convergence study provides us with a basis for reliable computation of eigen frequencies by the time-harmonic BEM.

The proposed BEM implementation combined with the IRAM eigenvalue solver provides a reliable platform for the computation of eigen frequencies for piezoelectric solids. It has a broader range of applications to the time-harmonic problems beyond the eigenvalue analysis.

Acknowledgments

Denda and Araki have performed the boundary element formulation, implementation and analysis. Yong and his graduate student Mr. Wei Wu performed the finite element formulation, implementation and analysis. Denda acknowledges discussions on the BEM formulation by Dr. C.Y. Wang of Schlumberger-Doll Research. Denda and Yong acknowledge the support by Seiko-Epson, Inc. Araki was supported by the grant-in-aid for scientific research No. (B)(2) 11209204 from the Ministry of Education, Culture, Sports, Science and Technology of Japan and No. (A) 13750540 from the Japan Society for the Promotion of Science.

References

Denda, M., Lua, J., 1999. Development of the boundary element method for 2D piezoelectricity. Composites B 30, 699–707.
Denda, M., Wang, C.Y., Yong, Y.K., 2003. 2-D time-harmonic BEM for solids of general anisotropy with application to eigenvalue problems. J. Sound Vibrat. 261, 247–276.
Kamiya, N., Andoh, E., Nogae, K., 1993. Eigenvalue analysis by the boundary element method. Eng. Anal. Boundary Elem. 12, 151–162.
Kitahara, M., 1985. Boundary Integral equation methods in Eigenvalue Problems of Elastodynamic and Thin Plates. Elsevier, Amsterdam.
Lekhnitskii, S.G., 1963. Theory of Elasticity of an Anisotropic Elastic Body. Hoden-Day, San Francisco.
Lehoucq, R.B., Sorensen, D.C., Yang, C., 1998. ARPACK User's Guide, SIAM, Philadelphia.
Moler, C.B., Stewart, G.W., 1973. An algorithm for generalized matrix eigenvalue problems. SIAM J. Num. Anal. 10 (2), 241–256.
Nardini, D., Brebbia, C.A., 1982. A new approach to free vibration analysis using boundary elements. In: Brebbia, C.A. (Ed.), Boundary Elem. Methods Eng.. Springer-Verlag, Berlin, pp. 312–326.
Norris, A.N., 1994. Dynamic Green's functions in anisotropic piezoelectric, thermoelastic and poroelastic solids. Proc. R. Soc. Lond. A 447, 175–188.
Stroh, A.N., 1958. Dislocations and cracks in anisotropic elasticity. Philos. Mag. 7, 625–646.
Wang, C.Y., Achenbach, J.D., 1994. Elastodynamic fundamental solutions for anisotropic solids. Geophys. J. Int. 118, 384–392.
Wang, C.Y., 1996. Green's functions and general formalism for 2D piezoelectricity. Appl. Math. Lett. 9 (4), 1–7.
Wang, J., Yong, Y.-K., Imai, T., 1999. Finite element analysis of the piezoelectric vibrations of quartz plate resonators with higher order plate theory. Int. J. Solids Struct. 36, 2303–2319.